Fabrication of three-dimensional nanostructures by focused ion beam milling

R. W. Tjerkstra[a)]
*Complex Photonic Systems (COPS) group, MESA$^+$ Institute for Nanotechnology, University of Twente,
P.O. Box 217, 7500 AE Enschede, The Netherlands*

F. B. Segerink
*Optical Sciences (OS) group, MESA$^+$ Institute for Nanotechnology, University of Twente, P.O. Box 217,
7500 AE Enschede, The Netherlands*

J. J. Kelly
*Condensed Matter and Interfaces group, Debye Institute, University of Utrecht, P.O. Box 80.000, 3508 TA
Utrecht, The Netherlands*

W. L. Vos
*Complex Photonic Systems (COPS) group, MESA$^+$ Institute for Nanotechnology, University of Twente,
P.O. Box 217, 7500 AE Enschede, The Netherlands and Center for Nanophotonics, FOM-Institute for Atomic
and Molecular Physics AMOLF, P.O. Box 41883, 1009 DB Amsterdam, The Netherlands*

The fabrication of an extended three-dimensional nanostructure with dimensions much larger than the feature size using a focused ion beam is described. By milling two identical patterns of pores with a designed diameter of 460 nm in orthogonal directions, a photonic crystal with an inverse woodpile structure was made in a gallium phosphide single crystal. The patterns are aligned with an unprecedented accuracy of 30 nm with respect to each other. The influence of GaP redeposition on the depth, shape, and size of the pores is described. A literature study revealed that the redeposition of GaP during milling is more pronounced than that of Si found in previous studies. An explanation for this phenomenon is given. © *2008 American Vacuum Society.* [DOI: 10.1116/1.2912079]

I. INTRODUCTION

Focused ion beam technology, developed in the 1970s as a derivative of ion beam implanting technology,[1–3] provides a very versatile tool that has been used for many different purposes. A surface can be modified with a finely focused beam because the ions (usually Ga$^+$) remove surface atoms, and hence the surface is milled. Because the technology does not require masks, it is ideal for (i) rapid prototyping;[4,5] (ii) modifying devices on which lithographic processes cannot be applied;[6] and (iii) the fabrication of highly specialized devices.[7] In practice, focused ion beam technology is mainly used for modifying computer chips, making transmission electron microscopy samples, and depositing metal layers for electrical connections.[3,8,9] Most of the applications described above require modification of the sample in two dimensions. However, in several fields of application the ability to fabricate three-dimensional structures by using a focused ion beam is highly advantageous, for instance for ultrahigh-resolution microscopy or for nanophotonics. One way of making three-dimensional structures is to vary the milling time of the beam as a function of its location.[10,11] In this way different depths in the sample can be achieved at different locations. If necessary, this method can be combined with tilting of the sample and milling from different directions. Thin membranes for examination in a transmission electron microscope[8] are routinely made using this method. The sample is usually tilted by approximately 2.5° during fabrication of the membrane to compensate for the numerical aperture of the focused ion beam.

By ion milling the sample from one direction, tilting the sample by a large angle, and then milling it from a second direction, extended and complicated three-dimensional structures can be made.[7,12] Schilling[13,14] and Wang[15,16] showed that large, three-dimensional structures in Si can be made by first etching in one direction using reactive ion etching, and subsequently milling in a second direction using a focused ion beam. In this paper we demonstrate that it is possible to make three-dimensional structures in GaP with dimensions on the order of 5 μm and feature sizes of 250 nm. The structures were fabricated exclusively using focused ion beam milling. We chose GaP because of its high index of refraction and large electronic gap, with a view to eventually making photonic crystals for the visible range. When made in a material with a high refractive index, photonic crystals can exhibit a photonic band gap: a frequency range in which light will not propagate because of multiple Bragg reflections.[17–19]

There are few alternative methods to focused ion beam milling in GaP, in contrast to Si, for which many different processing techniques have been developed.[13,20] This makes the study of the milling of GaP with a focused ion beam relevant. We have studied the differences between pores milled in bulk- and in porous material, and compare our results with those previously obtained for Si.[13,15,16] When three-dimensional structures with dimensions that are large

---

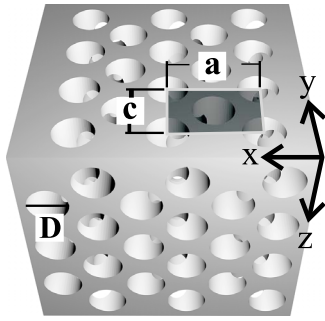[a)]Electronic mail: r.w.tjerkstra@utwente.nl

FIG. 1. Schematic drawing of an inverted woodpile photonic crystal structure. The $\vec{x}$, $\vec{y}$, and $\vec{z}$ directions are indicated. The crystal consists of two 2D lattices of pores that run in the $[110]$ and $[1\bar{1}0]$ crystallographic directions: the $\vec{y}$ and $\vec{z}$ pores, respectively. A unit cell of the 2D lattice is indicated, with lattice parameters a and c ($c=a/\sqrt{2}$). The pore diameter D is also indicated.
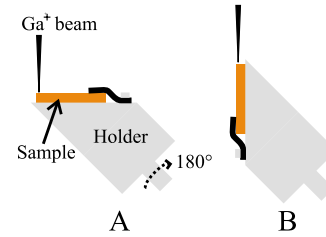

FIG. 2. The holder, used to rotate the samples in the focused ion beam, was made from aluminum, with a copper clip to hold the sample in place. For the milling of the first pattern (the $\vec{y}$ pores) the holder is placed in the position shown in (A). When the holder is rotated 180° (B) the other side of the sample is exposed to the beam and the second pattern (the $\vec{z}$ pores) can be etched.

compared to their smallest features have to be fabricated, the mutual alignment of the various parts poses a challenge. The orthogonal components are aligned with an accuracy better than 30 nm by using simple alignment marks. This is the first time a nanostructure was made by milling with FIB in two orthogonal directions and aligning the two patterns with respect to each other with very high precision using alignment marks.

II. EXPERIMENTAL METHODS

Gallium phosphide wafers were obtained from Marketech Inc. The wafers were (100) oriented, *n*-type, and S-doped, with a dopant density of $1-5\times10^{17}/cm^3$, specified by the manufacturer. Cleaving (100) wafers yielded samples with very smooth side walls that were (110) oriented. Focused ion beam milling was performed with an FEI Nova 600 dual beam apparatus that contained a focused Ga^+ ion- and electron beam column.

An inverted woodpile photonic crystal structure[14,21–23] was made by milling the same pattern of pores in two orthogonal directions in the GaP wafer. A schematic drawing of the inverted woodpile structure is shown in Fig. 1, with the important parameters: the diameter D of the pores, and the lattice parameters a and c of the two-dimensional lattice of pores that is milled in the two directions. The figure also defines the $\vec{x}$, $\vec{y}$, and $\vec{z}$ axes. Henceforth, we will call pores that run in the $\vec{y}$ direction the $\vec{y}$ pores, and the pores running in the $\vec{z}$ direction the $\vec{z}$ pores. The parameters of the inverted woodpile structure were chosen such that a photonic band gap would, in principle, be centered at wavelengths around 2000 nm. Therefore, the diameter D of the pores was 460 nm, and the lattice parameters were $a=958$ nm and $c=677$ nm. The thickness of the GaP walls between the pores is only 253 nm.

To investigate the influence of porosity on milling, we performed experiments both on bulk wafers and in slabs with a thickness below 2 μm. The diameter of the pores in bulk GaP was designed to be 483 nm. Since the best results were obtained with slabs, we now describe their fabrication.

To perform the milling in two orthogonal directions, the sample was mounted on a holder that held it at an angle of 45° with respect to the table of the focused ion beam apparatus; see Fig. 2. The assembly was mounted on the table, which was then tilted so that the sample was at an angle of 0° with respect to the ion beam [Fig. 2(A)].

In the first step of the fabrication process a slab was made by milling a large rectangular hole with an area of 7 $\times 11$ μm^2 and a depth of 3 μm at a distance of about 2 μm from the cleaved edge of the sample, with a current of 2.8 nA. The slab had two faces: the front face (the cleaved surface of the sample), and the back face (one of the walls of the rectangular hole). The back face of the slab was smoothened with the "polish mill" option of the focused ion beam apparatus, using a current of 98 pA. In this way a slab with the desired thickness of 1.7–1.9 μm could be made.

After the slab was formed, the sample holder was rotated by 180° [Fig. 2(B)]. The slab could now be milled in the $\vec{y}$ direction with the first hole pattern of the structure: the $\vec{y}$ pores. Automatic drift correction was applied during milling, using specially milled square markers. The beam current was 98 pA. In this way a two-dimensional crystal structure of 9 $\times 9$ unit cells with the parameters $D=460$ nm, $a=958$ nm, and $c=677$ nm was formed in the slab. In the next step, alignment marks consisting of two narrow lines with a width of approximately 50 nm and a spacing of 340 nm were milled in the side of the sample. The sample holder was again rotated by 180°.

A streamfile containing a cross-shaped pattern was drawn on the screen of the focused ion beam apparatus (see Fig. 3). The vertical bar of the cross was located exactly between the alignment marks on the sample, and the horizontal bar of the cross was aligned to the edge of the sample, as shown in the figure. In this way we achieved an alignment accuracy better than 30 nm. The streamfile that contained the second pattern of holes (shown as the circles in Fig. 3) was then placed at known distances to the first streamfile. The cross-shaped streamfile was then removed from the screen. In this way the $\vec{z}$ pores were milled parallel to the front face of the slab, perpendicular to the previously drilled pores, and in the desired places. All pores were milled simultaneously during the milling of a pattern of pores in either the $\vec{y}$ or $\vec{z}$ direction.
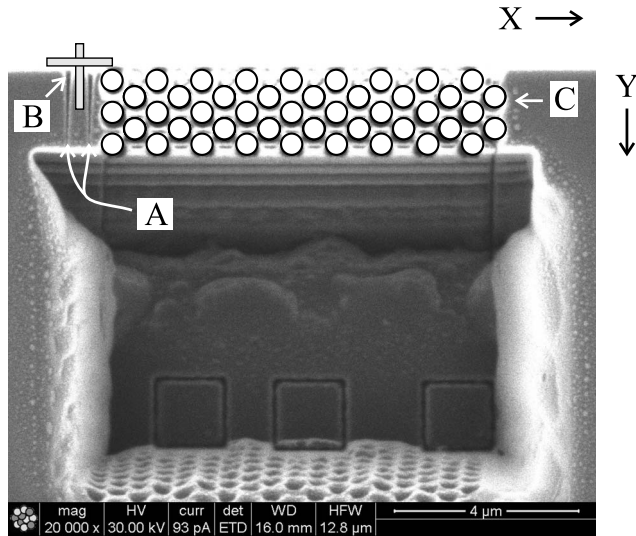
FIG. 3. Specially milled marks [the two vertical lines on the upper left corner of the sample, indicated by (A)] were used to align the two orthogonal patterns of pores. A streamfile containing a cross-shaped pattern [indicated by (B)] was drawn on the screen of the focused ion beam apparatus, and the vertical bar of the cross was located exactly between the alignment marks. In this way we achieved an alignment accuracy of approximately 30 nm in the $\vec{x}$ direction. The edge of the sample was aligned to the horizontal bar of the cross, as shown in the figure. The streamfile that contained the second pattern of holes [shown as the circles indicated by (C)] was then placed at known distances to the first streamfile.

Gas-assisted etching[24–26] using iodine was also investigated. The iodine reacts with the GaP, giving volatile particles and thus reducing redeposition.

After milling, scanning electron micrographs of the samples were made using the scanning electron microscopy (SEM) function of the dual beam apparatus. To investigate the tapering and depth of the pores, the porous slabs were opened using the "polish mill" function of the focused ion beam, to reveal the insides of the pores in the slab. The polish mill procedure removes very thin slices off the structure, thus minimizing the amount of redeposition. The diameters of the pores were measured as a function of the distance to the surface. All size measurements were done using a ruler and printed SEM pictures.

III. RESULTS AND DISCUSSION

Gas-assisted etching proved to etch the sidewalls of the pores to such an extent that they collapsed after a depth of approximately 100 nm was reached. Therefore, all subsequent experiments were done without gas-assisted etching.

A micrograph of the sample after formation of the porous slab (Fig. 4) clearly shows that the $\vec{y}$ pores perforate the slab completely, since the back wall of the hole also reveals pores. This observation shows that the tapering of the $\vec{y}$ pores was negligible. The marks used to align the two sets of pores with respect to each other are visible as two narrow parallel lines in the upper right-hand corner of the porous slab. The $\vec{z}$ pores are almost perfectly parallel to the front face of the slab. This alignment is very important for the quality of photonic crystals; if the angle between the two pore sets differs
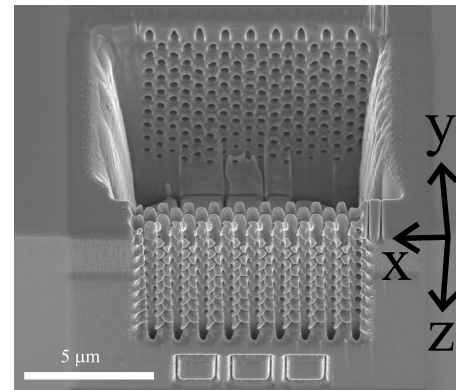

FIG. 4. SEM micrograph of a thin, three-dimensional photonic structure made in GaP using a focused ion beam. The structure is oriented in the same way as the structure in Fig. 1. The three squares underneath the slab are markers for the automatic drift correction. The two narrow lines on the right side of the slab are marks used to align the two orthogonal sets of pores with an accuracy of approximately 30 nm. The important parameters for the structure are $D=460$ nm, $a=958$ nm, and $c=677$ nm.

by more than 5° from the normal the photonic properties degenerate rapidly.[14] To the best of our knowledge, this is the first three-dimensional nanostructure that was made by consecutively aligning two orthogonally milled patterns with high precision.

Figure 5 shows the average diameter of all $\vec{z}$ pores as a function of the distance z from the top of the slab. Only a lower bound to the depth of the $\vec{z}$ pores could be determined; therefore, we can only give a minimum value of 13 for the obtainable aspect ratio in the $\vec{z}$ direction. We did not find any evidence of "channeling" of the ions in certain directions.[14]

Figure 5 also shows the average diameter of five pores made in bulk material as a function of the depth. The maximum depth of these pores was only 2.5 μm. The aspect ratio of pores made in bulk material is therefore limited to 2.8 ± 0.15. The limited depth and low aspect ratio are a consequence of the redeposition of sputtered material during
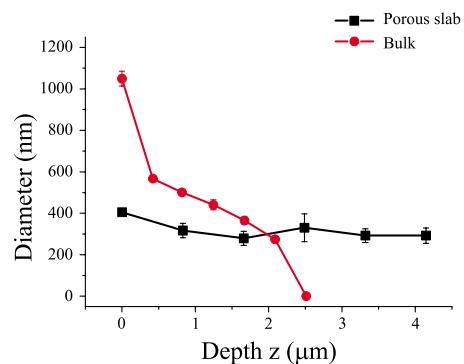

FIG. 5. Average diameter of all $\vec{z}$ pores in the slab as a function of the depth z inside the pore (connected squares). The average diameter of five pores made in bulk material as a function of the depth is shown as connected circles. The tapering of the pores in the slab is much less than that of the pores in bulk material.
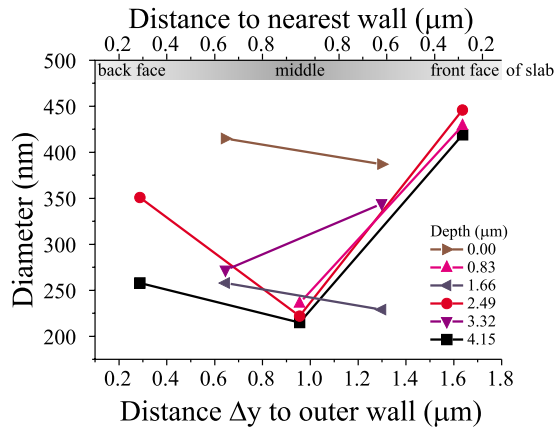
FIG. 6. Diameters of the $\vec{z}$ pores as a function of the distance Δy to the front face of the porous slab, and the depth z in the pore, measured from the top of the slab. The axis on top of the figure gives the distance of the pores to the nearest wall of the slab. Pores that are closer to one of the walls have a larger diameter than at the center of the slab.

FIG. 7. Average diameter of the $\vec{y}$ pores as a function of their distance z to the top of the porous wall (black squares). The average thickness of the redeposited layers inside the pores is also indicated (red circles).

milling. Consequently, focused ion beam milling of bulk wafers has limited capabilities compared to, for instance, wet or dry etching of bulk Si wafers.[13,20]

Because the $\vec{y}$ pores have to be made in bulk material in the first milling step, the thickness of the slab was chosen such that it could just be perforated (1.7–1.9 μm). When the slab was perforated the $\vec{y}$ pores could be milled to the correct diameter, and their tapering reduced to almost zero, because there were then two openings through which the sputtered material could escape. The reason why the tapering of the $\vec{z}$ pores in a porous slab is much less than in bulk material is that a porous slab has many openings through which sputtered material can escape.

The diameter of the pores made in bulk material decreased rapidly with depth at the top of the pore, close to the surface of the sample, and more slowly at distances further from the surface (Fig. 5, circles). In the slab, however, the diameter of the $\vec{z}$ pores is nearly constant over their whole length. Figure 5 shows that the average diameter of the $\vec{z}$ pores is approximately 300 nm, independent of the distance from the top of the slab. The walls between the pores are 413 nm thick. We observe that the pore diameter is significantly smaller than the designed value of 460 nm. This result is remarkable because the diameter of pores milled in this way is usually slightly larger than the designed diameter, due to beam- and stage drift. Here, stage drift is negligible, and the reduction in the diameter is caused by redeposition during milling.

To study the effect of redeposition, we plot in Fig. 6 the average diameter of a $\vec{z}$ pore as a function of its distance Δy from the front face of the porous slab. The axis at the top of Fig. 6 gives the distance of the pores to the nearest wall of the slab. The results clearly show that $\vec{z}$ pores close to the walls have a larger diameter than those at the center. The latter are surrounded by pores on all sides, whereas the former only have neighbors at one side. Material sputtered from pores near the walls has a higher chance of escaping the
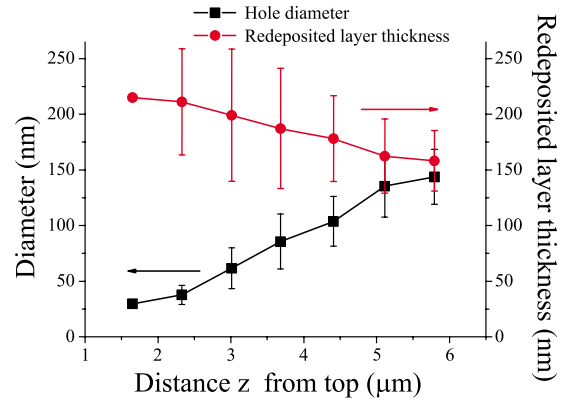
porous structure than material sputtered from pores at the center of the slab, and thus a lower chance of contributing to redeposition.

The $\vec{y}$ pores also suffer from redeposition during milling of the $\vec{z}$ pores. Figure 7 shows the final diameter of the $\vec{y}$ pores, measured after the $\vec{z}$ pores were milled, as a function of the distance z from the top of the wall. The thickness of the redeposited layer inside the pores was calculated on the basis of the initial diameter of the $\vec{y}$ pores (460 nm). The figure clearly shows that the pores located near the top of the wall have the smallest diameter (approximately 30 nm). With increasing depth, the pore diameter increases to approximately 140 nm, which is much smaller than the initial diameter of 460 nm. Figure 7 shows that the thickness of the redeposited layer in the pores decreases with depth from 220 to 160 nm. This result can be explained as follows: when the $\vec{z}$ pores are milled, they first penetrate the $\vec{y}$ pores closest to the top of the slab. These $\vec{y}$ pores suffer the most from redeposition because they are more exposed to sputtered material during milling. Redeposition of sputtered material during focused ion beam milling of GaP tends to deteriorate the quality of the final structures.

The papers on focused ion beam milling of porous Si by Schilling[13,14] and Wang,[15,16] and focused ion beam milling of vias in Si (Ref. 27) reveal no evidence of significant redeposition in Si. It should be noted that in the papers by Schilling and Wang, the first set of pores was made using a different technique (dry or wet etching). Nevertheless, it seems that redeposition is more severe in GaP than in Si. As an explanation, we pose the hypothesis that during milling, the surface of the GaP is covered in dangling bonds of P atoms. Positively charged particles that are removed from the GaP structure by the ion beam can easily attach to these dangling bonds, reforming bulk GaP.

IV. CONCLUSIONS

Three-dimensional nanostructures were created in single-crystal GaP wafers using focused ion beam milling in two orthogonal directions. A special holder was designed for the process. The two orthogonal patterns of pores were aligned

with an accuracy of approximately 30 nm. The highest aspect ratio of pores obtained in bulk GaP was 2.8 ± 0.15, which limits the maximum size of the three-dimensional structures. The maximum obtainable aspect ratio in porous material is much larger than 13. It is suggested that redeposition during fabrication of three-dimensional structures with a focused ion beam is more pronounced in GaP than in Si. Therefore, special measures must be taken to obtain structures with parameters close to their design specifications.

ACKNOWLEDGMENTS

[1] R. L. Seliger and W. P. Fleming, J. Appl. Phys. **45**, 1416 (1974).
[2] H. Yamaguchi, A. Shimase, S. Haraichi, and T. Miyauchi, J. Vac. Sci. Technol. B **3**, 71 (1985).
[3] J. Melngailis, J. Vac. Sci. Technol. B **5**, 469 (1987).
[4] P. Ekkels, R. W. Tjerkstra, G. J. M. Krijnen, J. W. Berenschot, J. Brugger, and M. C. Elwenspoek, Microelectron. Eng. **67–68**, 422 (2003).
[5] Y.-L. D. Ho, R. Gibson, C. Y. Hu, M. J. Cryan, J. G. Rarity, P. J. Heard, J. A. Timpson, A. M. Fox, M. S. Skolnick, M. Hopkinson, and A. Tahraoui, J. Vac. Sci. Technol. B **25**, 1197 (2007).
[6] L. A. Woldering, A. M. Otter, B. H. Husken, and W. L. Vos, Nanotechnology **17**, 5717 (2006).
[7] D. Iannuzzi, S. Daladi, V. Gadgil, R. G. P. Sanders, H. Schreuders, and M. Elwenspoek, Appl. Phys. Lett. **88**, 053501 (2006).
[8] S. Reyntjens and R. Puers, J. Micromech. Microeng. **11**, 287 (2001).
[9] T. Hoshino, K. Watanabe, R. Kometani, T. Morita, K. Kanda, and Y. Haruyama, J. Vac. Sci. Technol. B **21**, 2732 (2003).
[10] M. J. Vasile, Z. Niu, R. Nassar, W. Zhang, and S. Liu, J. Vac. Sci. Technol. B **15**, 2350 (1997).
[11] H. B. Kim, G. Hobler, A. Lugstein, and E. Bertagnolli, Nanotechnology **18**, 245303 (2007).
[12] T. H. Taminiau, F. B. Segerink, R. J. Moerland, L. K. Kuipers, and N. F. van Hulst, J. Opt. Soc. Am. A **9**, S315 (2007).
[13] J. Schilling and A. Scherer, Earth Interact. **3**, 90 (2005).
[14] J. Schilling, J. White, A. Scherer, G. Stupian, R. Hillebrand, and U. Gösele, Appl. Phys. Lett. **86**, 011101 (2005).
[15] K. Wang, A. Chelkonov, S. Rowson, P. Garoche, and J. M. Lourtioz, J. Phys. D **33**, L119 (2000).
[16] K. Wang, A. Chelkonov, S. Rowson, and J. M. Lourtioz, Appl. Phys. A: Mater. Sci. Process. **76**, 1013 (2003).
[17] E. Yablonovitch, Phys. Rev. Lett. **58**, 2059 (1987).
[18] E. Yablonovitch, J. Opt. Soc. Am. B **10**, 283 (1993).
[19] J. D. Joannopoulos, P. R. Villeneuve, and S. Fan, Nature (London) **386**, 143 (1997).
[20] L. A. Woldering, R. W. Tjerkstra, H. V. Jansen, I. D. Setija, and W. L. Vos, Nanotechnology **19**, 145304 (2008).
[21] K. M. Ho, C. T. Chan, C. M. Soukoulis, R. Biswas, and M. Sigalas, Solid State Commun. **89**, 413 (1994).
[22] R. Hillebrand, S. Senz, W. Hergert, and U. Gösele, J. Appl. Phys. **94**, 2758 (2003).
[23] S. Takahashi, M. Okano, M. Imada, and S. Noda, Appl. Phys. Lett. **89**, 123106 (2006).
[24] R. J. Young, J. R. Cleaver, and H. Ahmed, Microelectron. Eng. **11**, 409 (1990).
[25] R. J. Young, J. R. Cleaver, and H. Ahmed, J. Vac. Sci. Technol. B **11**, 234 (1993).
[26] T. Kosugi, K. Gamo, S. Namba, and R. Aihara, J. Vac. Sci. Technol. B **9**, 2660 (1991).
[27] V. Ray, N. Antoniou, N. Bassom, A. Krechmer, and A. Saxonis, J. Vac. Sci. Technol. B **21**, 2715 (2003).